SKB

TECHNICAL REPORT 88-03

Flow and solute transport in a single fracture. A two-dimensional statistical model

Luis Moreno[1], Yvonne Tsang[2], Chin Fu Tsang[2],
Ivars Neretnieks[1]

[1] Department of Chemical Engineering
Royal Institute of Technology
Stockholm, Sweden

[2] Earth Sciences Division
Lawrence Berkeley Laboratory
University of California
Berkeley, California, USA

January 1988

SVENSK KÄRNBRÄNSLEHANTERING AB
SWEDISH NUCLEAR FUEL AND WASTE MANAGEMENT CO

BOX 5864 S-102 48 STOCKHOLM
TEL 08-665 28 00 TELEX 13108-SKB

FLOW AND SOLUTE TRANSPORT IN A SINGLE FRACTURE, A TWO-DIMENSIONAL STATISTICAL MODEL

Luis Moreno[1], Yvonne Tsang[2], Chin Fu Tsang[2], Ivars Neretnieks[1]

1 Department of Chemical Engineering
Royal Institute of Technology
Stockholm, Sweden

2 Earth Sciences Division
Lawrence Berkeley Laboratory
University of California
Berkeley, California, USA

January 1988

FLOW AND SOLUTE TRANSPORT IN A SINGLE FRACTURE. A TWO-DIMENSIONAL STATISTICAL MODEL

Luis Moreno*
Yvonne Tsang+
Chin Fu Tsang+
Ivars Neretnieks*

January, 1988

*Department of Chemical Engineering
Royal Institute of Technology
100 44 Stockholm, Sweden.

+Earth Sciences Division
Lawrence Berkeley Laboratory
University of California
Berkeley, California 94720

SUMMARY

A two-dimensional model for a single fracture with variable apertures is presented. The spatial variation of the apertures in the fracture is defined by the aperture density distribution and the spatial correlation length. Flow and solute transport in the generated fractures are simulated. The simulated flow is unevenly distributed in the fracture and the flowrates may vary by several orders of magnitude. Cubic law fracture apertures are also calculated and are smaller than the mass balance fracture apertures. The pressure field in the fracture is calculated, in which great differences exist between this pressure and the pressure field for a fracture with constant aperture. The solute transport is studied using the particle tracking technique. Breakthrough curves for nonsorbing and sorbing species are simulated. The sensitivity of the two-dimensional model is studied by generating fractures with different parameters in the density distribution function, different correlation lengths, and different number of nodes used in one correlation length.

The flow is strongly reduced when the simulated normal stress is increased. The cubic law fracture aperture may be several orders of magnitude smaller than the mass balance fracture aperture.

CONTENTS

1. INTRODUCTION

In Sweden, crystalline rock has been selected as the most suitable bedrock in which to build a final repository for spent nuclear fuel. If a canister containing radioactive waste is breached, then water flowing in the bedrock will come in contact with the radioactive material. Since the only likely mechanism by which radionuclides could reach the biosphere is through groundwater transport in the fractured rock, it is important that the fluid flow and solute transport in a tight fractured rock are understood. The radionuclides may interact with the rock by means of sorption onto the surface of the fractures and by diffusion into the rock matrix and sorption onto the surfaces of the inner microfissures.

The current approaches to the problem of flow through a fractured medium can be classified into two broad categories: the equivalent porous medium approach and the discrete fracture approach. When the rock mass of interest contains many interconnecting fractures, it is appropriate to treat the fractured medium as an equivalent porous medium. In the porous medium approximation, the key parameters are the equivalent permeability tensor for fluid flow (Hsieh et al., 1985; Neuman et al., 1985) and the scale dependent dispersivity tensor for solute transport (Sauty et al., 1979; Gelhar et al., 1979; Pickens and Grisak, 1981).

For a tight fractured medium where the intersections of water bearing fractures are few, it is no longer a good approximation to define the entire fractured medium by averaged quantities such as the equivalent permeability tensor and the equivalent dispersivity tensor. Instead a discrete representation of the fractures has been used in the problem of flow (Long and Witherspoon, 1985; Long et al., 1982; Robinson, 1983) and solute transport (Schwartz et al., 1983; Smith and Schwartz, 1984; Endo et al., 1984; Rasmuson, 1985). In these cases the fracture is represented by a pair of parallel plates with a constant aperture.

However, based on theoretical and experimental studies on single fractures, the parallel−plate representation of the single fracture seems inadequate in the description of fluid movement through a fractured medium. The field experiments of solute migration in single fractures in the Stripa mine (Abelin et al., 1985; Neretnieks, 1985) showed that the parallel−plate assumption of a single fracture may be incorrect in describing the fluid movement through a single fracture. Abelin et al. (1985) found that the flow was very unevenly distributed along the fracture planes investigated and large areas did not carry any water. The channels made up only 5−20 % of the fracture plane. The nonsorbing tracers injected were unevenly transported through these channels. These facts present clear evidence of the channeling of flow within a single fracture.

Furthermore Abelin et al. also showed that the equivalent fracture aperture derived from the constant head permeability measurements was much smaller than the aperture derived from the tracer migration measurements. The migration measurements measured the residence volume of the tracer solution. The equivalent apertures obtained from these two different measurements should have been identical if the parallel−plate description of the fracture was valid.

Migration experiments were carried out in granitic rock at Cornwall (Heath, 1985). In the experiment two parallel boreholes were drilled to intersect a fracture. Between the set of boreholes, it was found that the flow connections varied considerably depending on where the holes intersected the fracture. The field experiment performed in a single fracture at the same site (Bourke, 1987) demonstrated that flow in a single fracture also took place in a limited number of channels. In this experiment five parallel holes were drilled in the fracture plane; each of the holes was pressurized in turn. The flows into the other holes were measured by means of packer tests. The measurements showed that flow took place in only a few channels and that the channels occupied a total area of about 10 % of the fracture plane.

Pyrak et al. (1985) performed laboratory experiments in which molten wood's metal was injected into single fractures of Stripa granite at different levels of applied normal stress. When the metal had cooled, the fractures were opened up and the formation of tortuous paths in single fractures was observed.

The relationship of fracture wall roughness to the fluid flowrate through a single fracture subject to normal stress has been analyzed in a series of theoretical papers (Tsang and Witherspoon, 1981, 1983; Tsang, 1984). The investigations show that only at low applied stress, when the fracture is essentially open, does the parallel−plate idealization adequately describe fluid flow. As the contact area between the fracture surfaces increases with stress, either applied or in situ, flow through a single fracture takes place in a few channels which are tortuous, have variable aperture along its length, and which may or may not intersect each other.

The results from field experiments, theoretical studies, and laboratory measurements as discussed above point to the fact that the parallel−plate idealization of a rock fracture fails to describe the fluid flow and solute transport in a single facture. In that approach the single fracture is defined by only the constant fracture aperture. However, the experimental results discussed above indicate that it is impossible to define an equivalent parallel−plate aperture consistent with the observed flow and transport phenomena. The flow through a rock fracture is clearly unlike that through a slit between smooth parallel−plates.

Channeling in a single fracture has been modeled considering a fracture formed by independent channels with different apertures (Neretnieks et al., 1982; Moreno et al., 1985). The individual channels were assumed to have constant aperture. Tsang and Tsang (1987) have recently proposed an alternate approach to the description of the flow and transport in a tight fractured medium. In their approach a number of tortuous channels with variable apertures along the channel lengths were used to describe flow through either a single fracture or a number of intersecting fractures.

In this report, we shall report on a detailed study of the flow and solute transport through a single fracture with variable apertures both in the main direction of the flow and in its perpendicular direction. The model will be extended to the study of flow and solute transport through a single fracture under stress.

2. THE CONCEPTUAL MODEL

From the point of view of flow and transport, a fracture is the aperture between the fracture surfaces. The fracture surfaces are rough and the aperture is not constant but varies spatially. There are areas where the two surfaces are in contact and the aperture is zero. In other areas the aperture increases to fractions of millimeters even in fractures under load. The spatial variation of the fracture aperture is characterized by the spatial correlation length. This means that within a range smaller than the correlation length the aperture values are more likely to be similar, but at separation distances larger than the correlation length there is little or no correlation between the aperture values.

It may be envisaged that the spatial correlation length of the aperture variation is scale dependent so that the spatial correlation length increases with the size of the fracture under study. There are some indications that this may be so in nature so that the flow and transport properties are controlled by the largest observed correlation length.

Fluid flowing through a fracture seeks out the least resistive pathways usually composed of the largest apertures. The main flow is therefore expected to occur through a few channels in the fracture plane. Zones with small apertures will usually have very little flow. Zones with large apertures do not necessarily have large flow because they may be isolated from the main flows by constrictions ocurring in the fracture.

The spatial variation of the apertures in the fracture is defined by an aperture density distribution, $n(\delta)$, and a spatial correlation length, λ. The fracture length in the direction of the main flow is L_x and in the direction perpendicular to it is L_y.

3. THE NUMERICAL MODEL

In this section we explain the method used for generating apertures in the fracture with a spatial correlation length, λ, and a given aperture density distribution, $n(\delta)$. The relationships used to calculate the flow through the single fracture will also be shown. Finally, we will describe the method used to calculate the solute transport through the fracture. Breakthrough curves for nonsorbing and sorbing tracers will be studied.

3.1 Generation of fracture apertures

The fracture plane is divided by a rectangular grid into nodes with different apertures. The number of nodes along the axes is determined by the ratio of correlation-length to length and by the number of nodes used to represent one correlation length.

The generation of the fracture apertures was performed using the code COVAR (Williams and El-Kadi, 1986) which was slightly modified. COVAR is a computer program for the generation of hydraulic conductivities when the distribution is normal or lognormal. The autocorrelated field of fracture apertures, in this case, is generated using the mean, the standard deviation, and an autocorrelation coefficient. Examples of generated grids are shown in Figures 2a-d.

3.2 Flow

For laminar conditions the flow through a channel with a constant aperture may be written as (Bird et al., 1960)

$$Q = \frac{1}{12} \frac{\delta^3}{\mu} W \frac{\Delta P}{\Delta L} \qquad (1)$$

where δ is the channel aperture, μ the dynamic viscosity, W the width of the channel, and $\Delta P/\Delta L$ the pressure gradient.

We assume that the aperture is very much smaller than the flow distance in the node so that the influence on pressure drop by the diverging or converging parts of the flow path is negligible. The flow between two adjacent nodes is determined by both apertures. Figure 1 shows a schematic diagram of the two adjacents nodes. The flow between nodes i and j may be expressed as

$$Q_{ij} = \frac{1}{6\mu} \frac{W}{L} \left[\frac{1}{\delta_i^3} + \frac{1}{\delta_j^3} \right]^{-1} (P_i - P_j) \qquad (2)$$

Equation (2) may be written as

$$Q_{ij} = \frac{(P_i - P_j)}{R} \qquad (3)$$

where

$$R = \frac{6 \mu L}{W} \left[\frac{1}{\delta_i^3} + \frac{1}{\delta_j^3} \right]$$

Mass balances may be written for each node. For node i the mass balance is

$$\sum_j Q_{ij} = 0 \qquad (4)$$

where Q_{ij}'s are the flows coming into or going out from node i.

Flow through the fracture is simulated by superimposing a pressure difference of 100 units from left to right over the generated grid. The upper and lower boundaries are closed so that no flow passes them. A system of equations (4) is then obtained for all nodes. The system of equations is solved using a routine to solve sparse linear equations (Numerical Algorithms Group, Library of Mathematical Routines). The solution for this system of equations yields the pressure at each node. Flow between adjacent nodes is then calculated using equation (3).

3.3 Solute transport

There are two main quantities which are of interest for solute transport: the mean residence time and the residence time distribution. The latter is often described by dispersion. There are several mechanisms which cause dispersion. In this context velocity variations are the most obvious. Other effects such as molecular diffusion, matrix diffusion, finite reaction rates, etc. will not be discussed here.

In our calculations, it is assumed that local dispersion within each channel is negligible, and that the overall dispersion in the fracture is caused only by the different residence times along different pathways.

The breakthrough curve is simulated using a particle-tracking technique (Schwartz et al., 1983; Robinson, 1984). A given number of particles is introduced in the known flow field at the fracture inlet. Particles coming to an intersection are distributed in the outlet channels with a probability proportional to the flowrates. Each individual particle is followed through the channel network. The mean residence time and variance may be used to determine the Peclet number, which is a dimensionless measure of the dispersivity. The dispersion may be expressed in terms of the spread in residence times, σ_t, of the breakthrough curve and is inversely proportional to the Peclet number, Pe

$$\frac{2}{Pe} = \sigma_t^2 / t'^2 \qquad (5)$$

where the mean residence time is

$$t' = \int_0^\infty \frac{c(\infty) - c(t)}{c(\infty)}\, dt \qquad (6)$$

and the variance of the residence time is

$$\sigma_t^2 = 2 \int_0^\infty t\, \frac{c(\infty) - c(t)}{c(\infty)}\, dt - t'^2 \qquad (7)$$

The residence time in a given node for nonsorbing tracers is determined by the total flow through the node and its volume

$$t_w = \frac{\text{node volume}}{\Sigma \text{ flow into the node}} \tag{8}$$

For sorbing tracers which are sorbed onto the surface of the fracture, a retardation factor may be defined

$$R_a = 1 + \frac{2\ K_a}{\delta} \tag{9}$$

where δ is the aperture of the node and K_a is the surface sorption coefficient. The residence time for the sorbing tracers is then deefined as $R_a \cdot t_w$.

4. RESULTS OF SIMULATIONS

Flow and solute transport calculations were carried out with this two-dimensional model for different realizations of the variable apertures in a single fracture. Fractures with specified aperture parameters were generated and the flow and solute transport properties of the generated fractures were studied. The generated fractures have the same mean aperture, but the standard deviation in the aperture density distribution (lognormal) and the ratio of correlation-length to length were varied. Another variable studied, which may influence the flow and transport, is the number of nodes used in the discretization of one correlation length.

4.1 Flow

The flowrates were calculated considering that each node, except on the borders, is connected to four adjacent nodes. A given pressure drop between the inlet and outlet was used (100 pressure units). Figures 3a-d show the flow for the fractures shown in Figure 2a-d. The flowrates vary by several orders of magnitude. The line thickness is proportional to the flowrate in the respective channel. Flowrates less than 0.2 % of the total flowrate through the fracture are not drawn.

From these results it is possible to observe that nodes with large apertures do not necessarily transmit large flowrates. Zones with larger apertures may have small flowrates if they are surrounded by nodes with small apertures. On the other hand, nodes with small apertures will mostly have low flowrates because the water will seek out other paths with lower resistance. In our case where we have assumed that locally the flow resistance is inversely proportional to the local aperture cubed, the impact of the aperture on the fluid flow is well manifested.

The flow properties are compared by means of flow through the fracture and the ratio δ_f/δ_c; the equivalent parallel-plate apertures derived from solute transport, δ_f; and the permeability measurements, δ_c. The flow properties of the fractures generated in the different realizations are shown in Table 1. For the mass balance fracture aperture, the mean and the minimum and maximum values are presented. For the ratio of mass balance aperture to permeability aperture, flowrate, and residence time, we used the median instead of the mean. The median was chosen because the large spread in the values render the mean a rather meaningless quantity. Appendix A shows, in detail, the results of the simulations.

For a perfectly planar fracture with smooth walls and constant aperture, only one value should be needed to define the fracture aperture. In fractures with a varying aperture this is not possible. If we are interested in the volume of the fracture, the mass balance fracture aperture, δ_f, may be used. On the other hand, δ_c, is the equivalent fracture aperture which would permit a certain flowrate at a given pressure drop, assuming laminar flow. It is based on the cubic law for flowrate which states that in a slit with laminar flow the flowrate is proportional to the aperture cubed, se equation (1). Because the flow is controlled by the small apertures along a flowpath, it is clear that $\delta_f > \delta_c$. In some in situ tracer tests the mass balance fracture aperture has been found to be 1 or 2 orders of magnitude greater than the permeability fracture aperture (Abelin et al., 1985). This is also confirmed by theoretical considerations (Tsang, 1984)

The "cubic law" fracture apertures, δ_c, were 2.1 times smaller than the mass balance fracture apertures, δ_f, for the realizations with $\sigma = 0.50$. For a standard deviation of 0.30 these values were 1.3−1.4. The ratio of δ_f/δ_c seems to be independent of the ratio of correlation length to flowpath length.

For a planar fracture with constant aperture and smooth walls, the pressure distribution is linear between the inlet and outlet. If the direction of the flow is along the x−axis, the relation between pressure and distance along the x−axis will be a straight line from P(inlet) to P(outlet), independent of the y−location. For fractures with variable aperture this relationship can not be used. Figures 4a and 4b show three pressure distributions for the fractures shown in Figures 2a and 2d. The pressure is shown versus the y−location for three x−locations: 0.25 L (solid line), 0.50 L (dashed line), and 0.75 L (chained line). For a fracture with constant aperture the curves would be three horizontal lines at 75, 50, and 25 units of pressure.

Great differences are observed between the pressure field for a fracture with constant aperture and a more realistic variable fracture aperture. Large pressure gradients are observed along the y−axis, this gradient should be zero for fractures with constant aperture. In the direction of the flow the pressure gradient is very different from the gradient calculated for a fracture with constant aperture. The pressure at a location in the fracture is principally determined by the way this point is connected to other locations and their respective flows. The pressure at a given point is closer to the pressure at locations connected by the channels with higher conductivity.

The fluid when it flows through a fracture seeks out the zones with lower resistivity. A few pathways (channels), where most of the flow takes place, may clearly be distinguished in the plane of the fracture (Figures 3a−d). To study the properties of

these "channels" 100 particles were introduced at the inlet and each particle was followed along the fracture. The particles were distributed among the inlet channels in proportion to the flowrates. The mean log aperture and the standard deviation for the aperture distribution along each pathway were determined assuming that the apertures in an individual pathway were also lognormally distributed. These values were averaged for the fastest (33 % of the pathways), the intermediate (34 % of the pathways), and the slowest pathways (33 % of the pathways) and are shown in Table 2.

In the next set of calculations we observe individual particles following a certain pathway during their transport through the fracture. Preferred pathways can only be identified by considering the paths of many particles or, as previously done, by determining the flowrate distribution.

For the fastest pathways the mean apertures are in the interval 108 to 180 μm (the mean aperture for the fractures were between 69 and 79 μm). The mean aperture, in general, is smaller for the slowest channels. The standard deviation in the aperture distribution is less for the fastest channels. The mean log−aperture showed smaller values for the slowest channels. This relationship is not very clear from the data shown in Table 2. The data show that the fastest pathways are characterized by a low standard deviation and the slowest channels by a smaller mean aperture. The standard deviation of the aperture distribution in a given pathway may be found in a wide interval (0.081−0.298, 0.114−0.346, and 0.115−0.338 for the fastest, intermediary, and slowest channels, respectively) representing pathways of very unequal characteristics. Figure 5 shows the density function for the apertures in the fracture and for the apertures in the fastest, intermediate, and slowest pathways for the fracture in Run 06. The three last curves were drawn using the average values for standard deviation and mean log−aperture. In this fracture the slowest channels show a low standard deviation and low log−aperture.

Tsang and Tsang (1987) described a model of nonintersecting channels with a variable aperture. All of the channels are determined using the same aperture density distribution − gamma distribution. In the present model the fracture apertures are generated using a lognormal distribution. The aperture along the flow channels of the generated fracture is characterized by a lower standard deviation and greater mean log−aperture than in the fracture aperture density distribution. The length of these channels was found to vary between 1.00 L and 1.95 L. Tsang and Tsang (1987) assumed that the nonintersecting channels had a length less than 2−3 L.

The above calculations were also used to determine the pressure variation along given channels. Some pressure profiles are presented in Figure 6 for the fracture in Run 06. Profiles A and B correspond to fast channels, profiles E and F correspond to slow channels, and the other ones to intermediate channels. The length of the channels has been normalized to 1.0. The gradients observed in these channels are very different from those in fractures with a constant aperture.

4.2 Solute transport

The breakthrough curves were determined using a particle tracking technique. The number of particles must be large enough to get an accurate determination of the residence time and Peclet number. Simulations were made with number of particles ranging from 100 to 6400 for a grid with 20 x 20 nodes. Breakthrough curves for different numbers of particles are shown in Figure 7. The resulting curves are very similar when 1600 or more particles are used in the simulations. The use of 200 to 400 particles was sufficient to get a rough estimation of the breakthrough curves and residence times.

Figure 8 shows the breakthrough curves for the fractures shown in Figures 2a−d. The transport properties for the different realizations are studied comparing the residence time and dispersion (Peclet number). The residence time may be calculated from the volume of the fracture and the flow through it. The residence time may also be determined from the breakthrough curves by the moment method, equation (6). The values determined by the moment method agree very well with the values determined from the fracture volume and flow through the fracture (Appendix A, Table A2).

The Peclet number may be calculated by means of moments, equation (5). The values determined using this equation yield unreliable values for fractures with high dispersion since σ_t is strongly influenced by the tail of the breakthrough curve. The Peclet number may be estimated from the arrival times for c/c_0 = 0.1, 0.5, and 0.9 (Neretnieks et al., 1982). From these arrival times the ratio $(t_{0.9}-t_{0.1})/t_{0.5}$ is determined and the Peclet number calculated from a curve of Pe versus $(t_{0.9}-t_{0.1})/t_{0.5}$ obtained from the solution of the Advection−Dispersion equation. This method does not take into account the part of the curve below 10 % and above 90 %. The Peclet number calculated using this relationship was larger than that calculated by means of moments, in most of the cases.

The Peclet number was in the interval 2.5−17.5 for transport through fractures generated with a standard deviation in the aperture distribution of 0.50. When a standard deviation of 0.30 was used the value of the Peclet number increased (8.5−42.0). Hence the dispersion is increased with an increase in the standard deviation of the aperture variation in the fracture. The ratio of correlation−length to flowpath length does not seem to influence the dispersion in the fracture significantly. A slight increase of the dispersion is observed when the ratio λ/L is increased. For breakthrough curves with low dispersion a good agreement is found between the Pe calculated by moments and the value calculated using the arrival times. The use of a very low ratio λ/L yields a fracture with a network of many interconnected channels. This situation implies a decrease of the dispersion of the breakthrough curve and more an approximation to the porous medium approach.

For a pulse injection at the inlet the breakthrough curve may be calculated by the number of particles that reach the outlet per unit of time. In this case the curve shows very large scattering. A great number of particles would be required to obtain a more smooth curve. The curve for a step injection is calculated by the cumulative number of particles which have reached the outlet at a given time, so the obtained curve is quite smooth. In practice, dispersion in each channel would also smooth the breakthrough curve. For a square pulse injection the breakthrough curve may be determined from the results for a step injection subtracting the same curve but delayed in time by the injection duration. Breakthrough curves obtained using different injection times (0.1, 0.25, 0.5, 1.0, and 2.0 times the residence time) are shown in Figure 9 for the fracture shown in Figure 2a.

4.3 Transport of sorbing tracers

Some preliminary calculations for sorbing tracers are presented below. For sorbing tracers the residence time in each node is a function of the fracture aperture, equation 9. Simulations were made for a sorbing species with a surface sorption coefficient of $8.0 \cdot 10^{-5}$ m. The fractures presented in Figures 2a−d were used. The retardation factor may be determined from the breakthrough curves as the ratio between the residence times for the sorbing and nonsorbing tracers. This value agrees very well with the value determined using the surface sorption coefficient and the mass balance fracture aperture in equation (9). For example, the retardation factor determined from the breakthrough curve for the fracture shown in run 06 is 3.34. The value obtained using δ_f in equation (9) is 3.30. For the other fractures the differences were also about 1 %. These simulations show that the retardation factor for sorbing species may directly be calculated from equation (9) if the mass balance aperture, δ_f, is used.

5. SENSITIVITY OF THE PARAMETERS

Ten realizations were made in each set, using the same values for the parameters for the generation of the fracture apertures. The arithmetic mean aperature was maintained constant by letting the value δ_o (the mean log aperture) given by

$$\delta_o = \bar{\delta}\, e^{-\frac{(\sigma\ \ell n\ 10)^2}{2}}$$

where $\bar{\delta}$ is the expected arithmetic mean aperture, δ_f. The arithmetic mean fracture aperture used in these simulations was 80 μm. A grid of 20 x 20 nodes was used in most of these calculations. The first set of fractures was generated using a standard deviation of 0.50 and a ratio of correlation length to length of 0.2. In the second set, a ratio λ/L of 0.1 was used. The third and fourth sets were generated using a standard deviation of 0.30. The λ/L ratios were 0.2 and 0.1, respectively, in these sets. The number of nodes used for representing one correlation length were 4 and 2 for λ/L ratios of 0.2 and 0.1, respectively. In the last sets the discretization was made using 2 and 4 nodes for one correlation length with λ/L ratios of 0.2 and 0.1, respectively. In these cases the grids were 10 x 10 and 40 x 40 nodes.

5.1 Dependence on different realizations

The variation of the flow and contaminant transport properties between different realizations within the same set of realizations were first studied.

Fracture apertures were generated using an arithmetic mean aperture of 80.0 μm. The resultant mean apertures (Table 1) in each realization vary from 56.3 to 145.0 μm for the realizations with a logarithmic standard deviation in the aperture density function of $\sigma = 0.50$. For $\sigma = 0.3$, the arithmetic mean fracture apertures, $\bar{\delta}$, were between 55.4 and 97.7 μm. The larger differences are shown when a greater standard deviation and greater ratio λ/L are used.

The most important variation between the different realizations within a same set of realizations was observed in the flowrates through the fracture. They were in the interval 35 to 1140 units of flow for the fractures generated using the larger standard deviation and the larger ratio of correlation length to length. This interval is reduced

from 38 to 318 units of flow if a ratio λ/L of 0.1 is used with the same standard deviation of $\sigma = 0.5$. On the other hand, for a standard deviation $\sigma = 0.3$ and ratio λ/L of 0.1 this interval is significantly smaller (244 to 533 units of flow). When a greater ratio of λ/L is used the interval is increased (155 to 948 units of flow).

A wide interval is also observed in the calculated water residence time (0.10 to 1.7 units of time). The variation between the minimum and maximum values are similar to the variations observed for the flowrate in the fracture. The water residence time is calculated from the fracture volume and flow through the fracture.

The ratio δ_f/δ_c shows smaller variations between the different realizations within a given set.

The interval of variation for the dispersion in solute transport is only influenced by the standard deviation.

From the statements above, it may be pointed out that in this kind of simulations a larger number of realizations would be carried out, in order to get reliable results, when a large standard deviation for the aperture distribution is used. The influence of the ratio of correlation length to length is in the same direction but less important.

5.2 Dependence on the standard deviation of the lognormal aperture distribution

Table 1 shows that the most important parameter in the generation of the fracture apertures is the standard deviation of the aperture distribution. For a large standard deviation the flow is decreased. The flowrates are about 75 and 340 units of flow for a standard deviation of 0.5 and 0.3, respectively. The ratio δ_f/δ_c is also larger when a larger standard deviation is used. These two relationships may be explained by the fact that a larger standard deviation means a greater number of small apertures. The small apertures strongly decrease the flow in these locations. On the other hand, the large apertures increase the flow in the fracture if they are connected directly. Otherwise they increase the residence time in the fracture but not the flowrate in it. If they are connected from one side of the fracture to the other, larger flow may be observed. Flowrates of above 1100 units of flow were calculated in the simulations.

The dispersion of the solute transport is increased when a larger standard deviation is used. The Peclet number is about 8 for a standard deviation of 0.50. When the standard deviation is 0.30 the Peclet number is about 20. This shows the strong influence of the aperture density distribution used in the generation of the fracture on the dispersion of tracers flowing through it. In this model we assumed that the dispersion is due only to channeling effects. This means that for a very small standard deviation the dispersion is negligible. In the limit, if the standard deviation is zero, then the dispersion is zero also in our model (plug flow in the fracture).

5.3 Dependence on the ratio of correlation length to transport length

The results show that for a low ratio of λ/L, e.g. $\lambda/L = 0.10$, the dispersion of the tracer in the fracture is slightly reduced. The use of a very low ratio for λ/L yields a fracture with a network of many interconnected channels. This implies a decrease of the dispersion of the breakthrough curve due to channeling and an approximation to the porous medium approach.

The hydraulic properties of the fracture are slightly modified. For a large ratio of λ/L the total flow in the fracture and the ratio δ_f/δ_c seem to be slightly reduced. But the maximum values obtained for the flowrate in the fracture and the ratio λ/L are higher. These results could be explained by the greater possibility of the fluid to find channels connecting inlet and outlet through large fracture apertures.

5.4 Dependence on discretization of each correlation length

In the cases shown above, grids of 20 x 20 nodes were used. This means that for a ratio λ/L of 0.2, 4 nodes were used in the discretization of a correlation length. For a ratio λ/L of 0.1, the number of nodes was 2 in each correlation length. In the first set of realizations we used a ratio λ/L of 0.2 and only 2 nodes in each correlation length (Table 1, runs 40−49). The results are similar to the results obtained using 4 nodes in a correlation length (Table 1, runs 00−09). Dispersion seems to show a larger interval of variation. In the next set, 4 nodes per correlation length were used to simulate a fracture with a ratio λ/L of 0.1. In this case the results for runs 50−59 also agree well with the results of runs 10−19 in which only 2 nodes are used.

The use of a grid of 40 x 40 required the utilization of a computer with a large memory. The time of computation is strongly increased. A grid of only 10 x 10 is enough to get a estimation of the flow and solute transport properties. We propose that the use of grid 20 x 20 nodes is an adequate solution.

6. FLOW AND SOLUTE TRANSPORT IN A SINGLE FRACTURE UNDER NORMAL STRESS

In the model presented in this report the fracture aperture is never zero. For the realization shown in Figure 2a fracture apertures are in the interval 1.3−1,070 μm for a fracture with standard deviation σ = 0.50. When a smaller standard deviation (σ = 0.30) is used the interval is 5.6−499 μm. In practice, the zones of the fracture with a small aperture, e.g. smaller than 5−10 μm, have a very low flow due to the assumption used here that the flow is proportional to the aperture cubed.

When the fracture is subjected to normal stress the fracture surfaces are put in contact and the fracture is closed in these zones. If the normal stress is increased the contact points or zones will be deformed and increased and new contact zones will be created.

When no stress acts on the fracture, the fluid in the fracture flows through certain preferential channels due to the aperture variation as shown in Figures 3a−d. When normal stress is applied on the fracture the small apertures will be reduced or closed. This implies that the small channels will disappear and the fluid will only flow through the largest channels. Thus the larger the normal stress, the larger is the channeling effect. A very high normal stress may totally stop the flow in the fracture even when the fracture is not closed everywhere because there is no connection between the open portions.

Two different realizations were tested. One of the realizations was the fracture in Run 06, which was obtained using a high standard deviation in the lognormal distribution (σ = 0.50). The other one had a standard deviation of 0.30, fracture in Run 25.

Flow and solute transport were calculated for decreases of the fracture aperture by 2, 4, 8, 16, and 24 μm. The flow and transport properties of the resulting fractures are shown in Table 3. The flow in the fracture is decreased when the fracture aperture is reduced, i.e. with an increase of the normal stress. For small decreases of fracture aperture (i.e. low normal stress) the variations of the flowrate are small. But for decreases larger than 16 μm, the flowrate is strongly reduced and the dispersion in the fracture is increased. For a high aperture reduction the Peclet number is low or very low.

The simulation made on a fracture generated using a low standard deviation shows a smaller influence from the decrease of the fracture aperture or applied normal stress. The cause of this is that for the fracture with $\sigma = 0.30$, the smallest aperture is 5.6 μm. Surface contact is reached only when $\Delta\delta$ is greater than 5.6 μm.

When the normal stress is increased the contact area in the fracture is increased. For the fracture with $\sigma = 0.50$ this contact area is 15 % for an aperture decrease of 16 μm. For the fracture with $\sigma = 0.30$ the contact area is 1.8 %, and due to this reason a simulation was also made using an aperture decrease of 32 μm. For this new aperture the contact area is 15 %. Laboratory experiments on granite cores (Pyrak−Nolte et al., 1987) show that contact area ranges from 8 − 15 % at a normal stress of 3 MPa. When the aperture is decreased by the applied normal stress the aperture density distribution is modified. The lognormal distribution does not allow for apertures equal to zero. Therefore all the apertures in the fractures with a value less than 1 μm were eliminated and the parameters in the new density distribution were calculated. In both cases the standard deviation in the aperture distribution is increased. This variation is more important for the fracture with an original standard deviation of 0.30. The standard deviation increased from 0.43 to 0.55 and from 0.30 to 0.48 for the fractures in runs 06 and 25, respectively, for a aperture reduction of 24 μm.

7. DISCUSSION

With the two−dimensional model, we may qualitatively show that the variation in aperture in a single fracture has the effect that most of the fluid flows through a few pathways − the flow is channeled. This has been observed in several laboratory and in situ experiments. Moreover, the dispersion which occurs in the fracture may, to a large extent, be accounted for by channeling. The use of this model for a quantitative description of flow and solute transport is limited to finding the expected values for water flow in the fracture, residence time, and dispersion. A given simulation only represents one of the infinite number of possible realizations.

When the model is applied to a study of a fracture in the laboratory, e.g. a fracture with the size 10 x 10 cm, the apertures may be measured (Pyrak et al., 1985). From these measurements the standard deviation and the mean log aperture in the aperture density distribution and the correlation length could be determined. The use of this model for longer distances implies that the ratio λ/L must change. For long distances λ/L will become very small and it may then be expected that the number of channels will increase. The situation will approach a two dimensional porous medium. It is then implicitly assumed that the correlation length λ is a constant independent of scale. This may not be the case. In the porous medium approach a scale dependent dispersivity has been used in large scale experiments (Pickens and Grisak, 1981). For fractured media Neretnieks (1985) has sampled data from different tracer test and has shown that the dispersivity in fractured media is increased with the distance of the experiment. A dispersivity of about 0.1 L (Pe = 10) was obtained. To extend this model from laboratory experiments to in situ experiments we may assume that the correlation length is directly related to the distance used in the in situ experiments. The same standard deviation in the aperture density distribution would be used. This implies that the scale of the irregularities in the fracture would be increased. In large scale tracer tests, great irregularities (e.g. great channels) would be included. When we change to a smaller scale these great irregularities would be excluded from the actual fracture. If one of these great irregularities is included in the fracture, the correlation length would be about L, i.e. $\lambda/L \approx 1$. How to define or measure the correlation length and the parameters in the aperture density distribution are problems that must be studied in more detail.

In this report we have studied flow and solute transport in a fracture with a variable aperture for some values of the parameters. To get quantitative results from this model a large number of realizations must be made. The expected values for flow through the fracture, the ratio δ_f/δ_c, and the dispersion of the breakthrough curves could be adequate parameters to characterize the flow and transport properties of the fracture or

fractured medium. These expected values could be expressed as a function of the aperture density distribution (δ_0 and σ), the ratio λ/L, the normal stress, and other factors (e.g. presence of filling material).

As a motivation for further development of this model some simulations are compared with experimental tracer test. Figures 10 and 11 show two tracer test with the nonsorbing tracer NaLS performed in the laboratory by Eriksen and coworkers (1985). The tracer tests were carried out in a natural fracture in a granitic drill core. The dimensions of the drill core were 187 mm in length and 88 mm in diameter. Figures 10 and 11 demostrate the potential capability of the model to reproduce experimental data.

NOTATION

c	Concentration in the fluid	M/L^3
c_o	Concentration in the fluid at the inlet	M/L^3
K_a	Surface sorption coefficient	L
L	Length	L
P	Pressure	M/LT^2
Pe	Peclet number	
Q	Flowrate	L^3/T
W	Channel width	L
R	Resistance	M/L^4T
R_a	Surface retardation factor	
t_w	Water residence time	T
$t_{0.1}$	Arrival time for $c/c_o = 0.1$	T
$t_{0.5}$	Arrival time for $c/c_o = 0.5$	T
$t_{0.9}$	Arrival time for $c/c_o = 0.9$	T
δ	Channel aperture	L
δ_o	Mean log aperture	L
δ_c	Cubic law fracture aperture	L
δ_f	Mass balance fracture aperture	L
$\overline{\delta}$	Arithmetic mean fracture aperture	L
λ	Correlation length	L
μ	Dynamic viscosity	M/LT
σ	Standard deviation in the lognormal distribution	
σ_t	Standard deviation in the breakthrough curve.	

REFERENCES

Abelin, H., I. Neretnieks, S. Tunbrant, and L. Moreno, Migration in a single fracture: Experimental results and evaluation, final report, Stripa project, Stockholm, Sweden, May 1985.

Bear, J., Dynamics of fluids in porous media, 764 pp., Elsevier, New York, 1972.

Bird, R.B., W.E. Stewart, and E.N. Lightfoot, Transport Phenomena, John Wiley, New York, 1960.

Bourke, P.T., Channeling of flow through fractures in rock, Proceedings of GEOVAL − 87, Internatinal Symposium, Stockholm, Sweden, April 7−9, 1987.

Endo, H.K., J.C.S. Long, C.R. Nilson, and P.A. Witherspoon, A model for investigating mechanical transport in fracture networks, Water Resour. Res., 20 (10), 1890−1400, 1984.

Engelder, T. and C.H. Scholz, Fluid flow along very smooth joints at effective pressure up to 200 megapascals, in Mechanical Behavior of Crustal Rocks, Geophys. Monogr., Vol. 24, edited by N.L. Carter, et al., pp. 147−152, AGU, Washington, D.C., 1981.

Eriksen, T.E., Migration in single fissures, SKB progress report, May, 1985.

Gelhar, L.W., A.L. Gutjahr, and R.L. Naff, Stochastic analysis of macro dispersion in a stratified aquifer, Water Resour. Res., 15(6), 1387−1397, 1979.

Hsieh, P.A., S.P. Neuman, G.K. Stiles, and E.S. Simpson, Field determination of three−dimensional hydraulic conductivity tensor of anisotropic media, 2, Methodology and application to fractured rock, Water Resour. Res., 21(11), 1667−1676, 1985.

Heath, M.J., Solute migration experiments in fractured granite, South West England., in Design and instrumentation of in situ experiments in underground laboratories for radioactive waste disposal, Proceedings of a joint CEC−NEA workshop, Brussels, 15−17 May 1984, pp 191−200. Edited by Balkema, Netherlands, 1985.

Levenspiel, O., Chemical Reaction Engineering, 2nd ed., Wiley International Ed., New York, 1972.

Long, J.C.S., J.S. Remer, C.R. Wilson, and P.A. Witherspoon, Porous media equivalent for networks of discontinuous fractures, Water Resour. Res., 18(3), 645−658, 1982.

Long, J.C.S. and P.A. Witherspoon, The relationship of the degree of interconnection to permeability of fracture networks, J. Geophys. Res., 90(B4), 3087−3098, 1985.

Moreno, L., I. Neretnieks, and T. Eriksen, Analysis of some laboratory tracer runs in natural fissures, Water Resour. Res., 21(7), 951−958, 1985.

Neretnieks, I., Transport in fractured rocks, Proceedings, Memoires of the 17th International Congress of IAH, Tucson, AZ, Vol. XVII, 301−318, 1985.

Neretnieks, I., T. Eriksen, and P. Tähtinen, Tracer movement in a single fissure in granitic rock: some experimental results and their interpretation, Water Resour. Res., 18(4), 849−858, 1982.

Neuman, S.P., E.S. Simpson, P.A. Hsieh, J.W. Jones and C.L. Winter, Statistical analysis of hydraulic test data from fractured crystalline rock near Oracle, Arizona, Proceedings, Memoires of the 17th International Congress of IAH, Tuscon, AZ, 289−301, 1985.

Pickens, J.F. and G.E. Grisak, Modeling of scale−dependent dispersion in hydrologic systems, Water Resour. Res., 17(6), 1701−1711, 1981.

Pyrak, L.R., L.R. Myer, and N.G.W. Cook, Determination of fracture void geometry and contact area at different effective stress, Transactions, American Geophysical Union, 66(903), 1985.

Pyrak−Nolte, L.J., L.R. Myer, N.G.W. Cook, and P.A. Witherspoon, Hydraulics and mechanical properties of natural fractures in low permeability rocks, proceedings of Sixth International Rock Mechanical Symposium, Montreal (in press).

Rasmuson, A., Analysis of hydrodynamic dispersion in discrete fracture networks using the method of moments, Water Resour. Res., 21(11), 1677−1683, 1985.

Robinson, P.C., Connectivity of fracture systems − a percolation theory approach, J. Phys. A: Math. Gen., 16, 605−614, 1983.

Robinson, P.C., Connectivity, flow and transport in network models of fractured media, Ph.D. Thesis, Oxford University, Oxford, 1984.

Sauty, J−P., A.C. Gringarten, and P.A. Landel, The effect of thermal dispersion on injection of hot water in aquifers, paper presented at the second invitational Well Testing Symposium, U.S. Dept. of Energy, Lawrence Berkeley Laboratory, Berkeley, CA, 1979.

Schwartz, F.W., L. Smith, and A.S. Crowe, A stochastic analysis of macroscopic dispersion in fractured media, Water Resour. Res., 19(5), 1253−1265, 1983.

Smith, L. and F.W. Schwartz, An analysis of the influence of fracture geometry on mass transport in fractured media, Water Resour. Res., 20(9), 1241−1252, 1984.

Tsang, Y.W., The effect of tortuosity of fluid flow through a single fracture, Water Resour. Res., 20(9), 1209−1215, 1984.

Tsang, Y.W. and C.F. Tsang, Channels model of flow through fractured media, Water Resour, Res., 23(3), 467−479, 1987.

Tsang, Y.W. and P.A. Witherspoon, Hydromechanical behavior of a deformable rock fracture subject to normal stress, J. Geophys. Res., 86(B10), 9287−9298, 1981.

Tsang, Y.W. and P.A. Witherspoon, The dependence of fracture mechanical and fluid properties on fracture roughness and sample size, J. Geophys. Res., 88(B3), 2359−2366, 1983.

Williams, S.A. and A.I. El−Kadi, COVAR − A computer program for generating two−dimensional fields of autocorrelated parameters by matrix decomposition, International Groundwater Modelling Center, Holcomb Research Institute, Butler University, Indianapolis, ID, 1986.

Table 1

Flow and transport properties for different realizations.

Runs	σ	δ_o	λ/L	n
00-09	0.50	41.2	0.20	4

		Mean	Median	Minimun	Maximum
δ_f, μm		78 ± 28		56.32	145.0
δ_f/δ_c		2.1 ± 0.4	2.05	1.66	3.15
Flow(1),	L^3/T		72.5	34.81	1 141
tw(1,2),	T		0.98	0.127	1.739
Pe(3)			4.3	1.38	8.29
Pe(4)			6.4	2.5	17.5

Runs	σ	δ_o	λ/L	n
10-19	0.50	41.2	0.10	2

		Mean	Median	Minimun	Maximum
δ_f, μm		78 ± 11		57.34	90.60
δ_f/δ_c		2.1 ± 0.2	2.15	1.67	2.48
Flow(1),	L^3/T		81.4	37.95	317.5
tw(1,2),	T		0.92	0.285	1.511
Pe(3)			6.0	0.86	11.63
Pe(4)			10.8	4.1	15.5

Table 1 (cont.)

Runs	σ	δ_o	λ/L	n
30-39	0.30	63.0	0.20	4

		Mean	Median	Minimun	Maximum
δ_f, μm		76 ± 12		55.40	97.68
δ_f/δ_c		1.3 ± 0.1	1.29	1.20	1.50
Flow(1),	L^3/T		336.3	154.7	947.7
tw(1,2),	T		0.22	0.103	0.358
Pe(3)			13.0	9.35	26.95
Pe(4)			19.3	8.5	33.5

Runs	σ	δ_o	λ/L	n
20-29	0.30	63.0	0.10	2

		Mean	Median	Minimun	Maximum
δ_f, μm		77 ± 6		66.69	84.98
δ_f/δ_c		1.4 ± 0.1	1.37	1.27	1.46
Flow(1),	L^3/T		359.5	243.9	533.4
tw(1,2),	T		0.22	0.158	0.299
Pe(3)			21.8	9.12	43.36
Pe(4)			21.0	9.0	42.0

Table 1 (cont.)

Runs	σ	δ_o	λ/L	n
40-49	0.50	41.2	0.20	2

		Mean	Median	Minimun	Maximum
δ_f, μm		80 ± 24		46.95	114.7
δ_f/δ_c		2.0 ± 0.4	2.17	1.13	2.56
Flow(1),	L^3/T		106.0	13.16	1 166
tw(1,2),	T		0.75	0.081	3.568
Pe(3)			4.1	0.18	12.21
Pe(4)			14.8	3.0	26.0

Runs	σ	δ_o	λ/L	n
50-59	0.50	41.2	0.10	4

		Mean	Median	Minimun	Maximum
δ_f, μm		74 ± 10		58.57	92.83
δ_f/δ_c		2.2 ± 0.4	2.06	1.65	2.97
Flow(1),	L^3/T		94.6	15.30	358.2
tw(1,2),	T		0.89	0.259	3.828
Pe(3)			5.4	3.17	12.47
Pe(4)			6.0	2.6	16.6

(1) Arbitrary units

(2) Calculated from fracture volume/flow

(3) Calculated using moments

(4) Calculated from $(t_{0.9}-t_{0.1})/t_{0.5}$

Table 2

Aperture distribution in individual pathways in some fractures.

Run	06	18	34	25
For generation:				
mean aperture, μm	80.0	80.0	80.0	80.0
standard deviation	0.50	0.50	0.30	0.30
mean logaperture	41.2	41.2	63.0	63.0
ratio λ/L	0.20	0.10	0.20	0.10
Actual fracture:				
mean aperture, μm	69.4	71.6	75.3	78.8
standard deviation	0.43	0.47	0.28	0.30
Channels:				
The fastest:				
mean aperture, μm	180	120	108	110
standard deviation	0.20	0.24	0.11	0.09
mean logaperture	116	89	98	98
The intermediate:				
mean aperture, μm	176	142	103	104
standard deviation	0.22	0.31	0.11	0.12
mean logaperture	111	97	90	91
The slowest:				
mean aperture, μm	92	128	102	105
standard deviation	0.20	0.33	0.13	0.16
mean logaperture	67	81	85	87
Channel length				
minimum, L	1.05	1.00	1.00	1.00
maximum, L	1.80	1.95	1.75	1.80

Table 3

Flow and transport properties in a single fracture under normal stress.

Fracture generated with σ= 0.50, δ_o= 41.2 μm, and λ/L= 0.20

Run	$\Delta\delta$ μm	Contact Area	δ_f μm	δ_f/δ_c	Flow(1) L^3/T	tw(1) T	Pe(2)
06	0.0	No	69.41	1.95	90.49	0.76	6.0
60	2.0	No	67.41	2.03	73.21	0.93	5.5
61	4.0	0.01	65.41	2.12	58.67	1.11	4.5
62	8.0	0.04	61.52	2.33	36.60	1.64	4.0
63	16.0	0.15	54.30	2.99	11.96	4.31	3.0
64	24.0	0.28	48.11	4.54	2.38	27.60	3.5

Fracture generated with σ= 0.30, δ_o= 63.0 μm, and λ/L= 0.10

Run	$\Delta\delta$ μm	Contact Area	δ_f μm	δ_f/δ_c	Flow(1) L^3/T	tw(1) T	Pe(2)
25	0.0	No	78.83	1.37	377.6	0.21	23.0
65	2.0	No	76.83	1.39	335.1	0.23	21.5
66	4.0	No	74.83	1.42	295.4	0.26	18.0
67	8.0	0.01	70.83	1.46	226.5	0.31	13.0
68	16.0	0.02	62.92	1.59	124.0	0.50	6.0
69	24.0	0.07	55.25	1.77	60.7	0.88	5.5
70	32.0	0.15	48.14	2.06	25.5	1.73	5.8

(1) Arbitrary units

(2) Calculated from $(t_{0.9}-t_{0.1})/t_{0.5}$

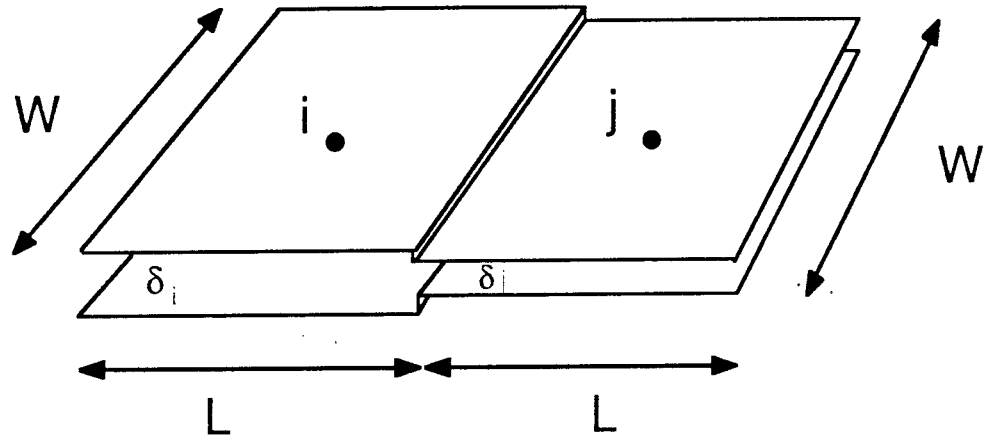

Figure 1 A schematic drawing of two adjacent nodes.

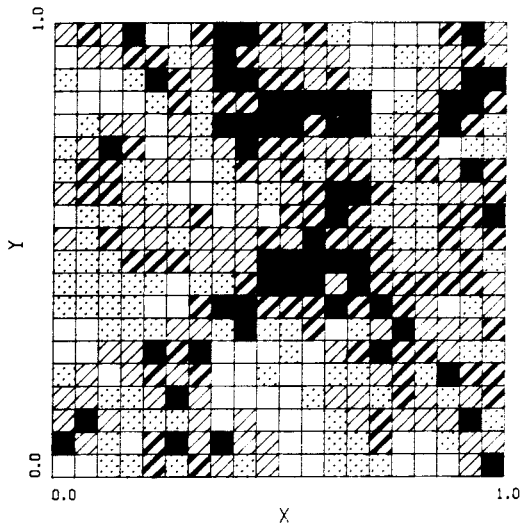

Figure 2a Fracture apertures generated using $\sigma = 0.50$, $\delta_o = 41.2$ μm, and $\lambda/L = 0.20$ (Run 06). The black nodes represent the smallest apertures and the white nodes the greatest apertures.

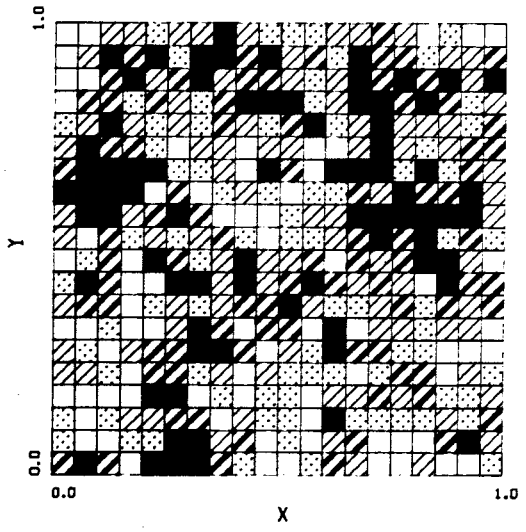

Figure 2b Fracture apertures generated using $\sigma = 0.50$, $\delta_o = 41.2$ μm, and $\lambda/L = 0.10$ (Run 18). The black nodes represent the smallest apertures and the white nodes the greatest apertures.

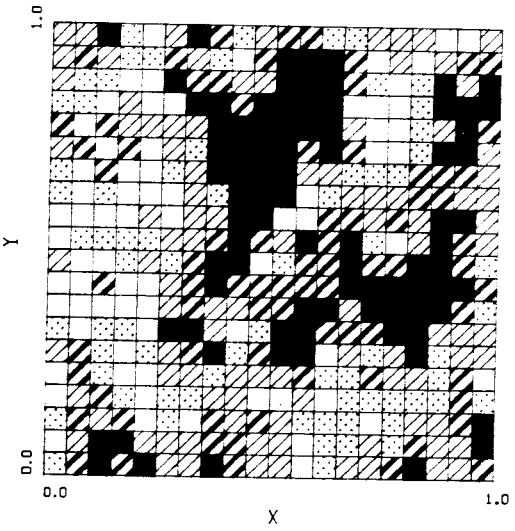

Figure 2c Fracture apertures generated using σ = 0.30, δ_o = 63.0 μm, and λ/L = 0.20 (Run 34). The black nodes represent the smallest apertures and the white nodes the greatest apertures.

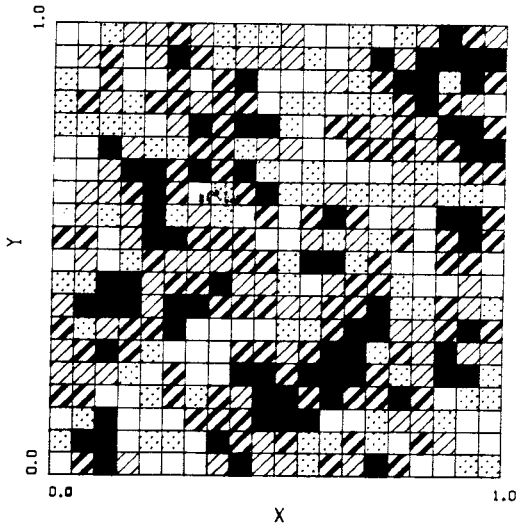

Figure 2d Fracture apertures generated using σ = 0.30, δ_o = 63.0 μm, and λ/L = 0.10 (Run 25). The black nodes represent the smallest apertures and the white nodes the greatest apertures.

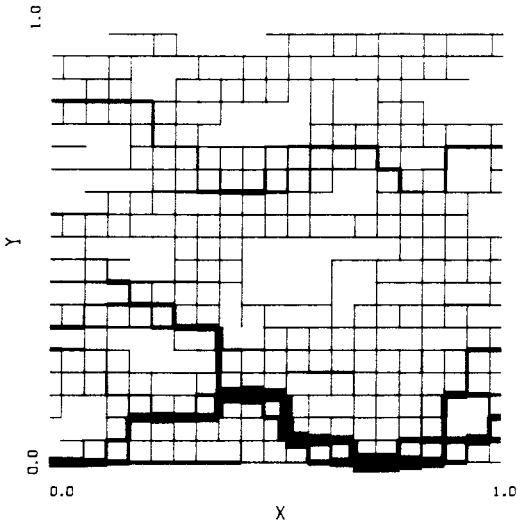

Figure 3a Fluid flow in the fracture for Run 06. The line thickness is proportional to the flow. Flows less than 0.2% of the total flow are not drawn.

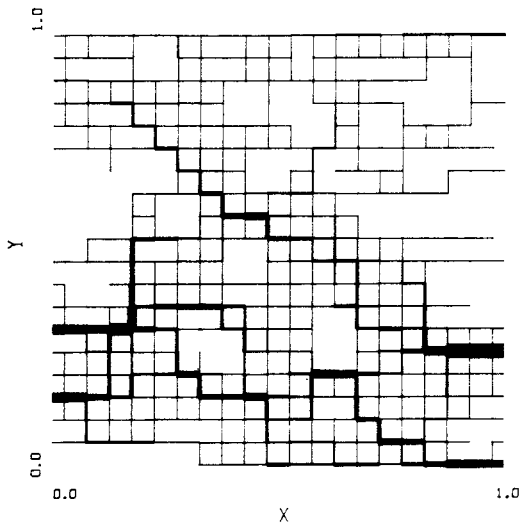

Figure 3b Fluid flow in the fracture for Run 18. The line thickness is proportional to the flow. Flows less than 0.2% of the total flow are not drawn.

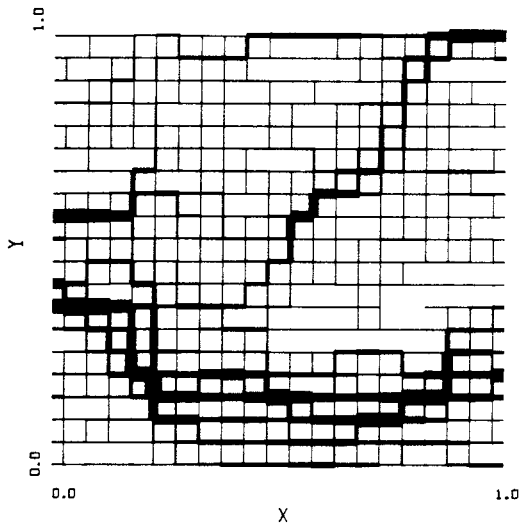

Figure 3c Fluid flow in the fracture for Run 34. The line thickness is proportional to the flow. Flows less than 0.2% of the total flow are not drawn.

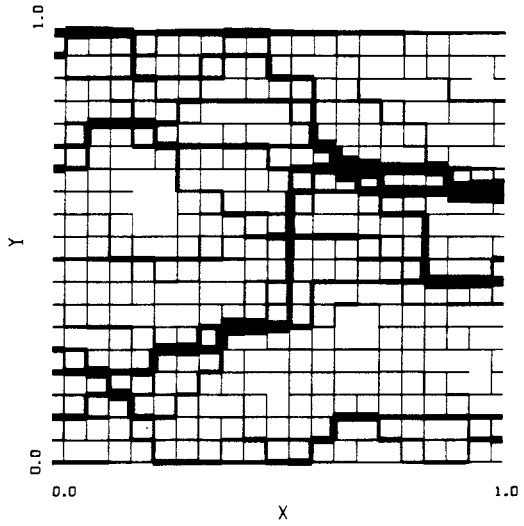

Figure 3d Fluid flow for the fracture for Run 25. The line thickness is proportional to the flow. Flows less than 0.2% of the total flow are not drawn.

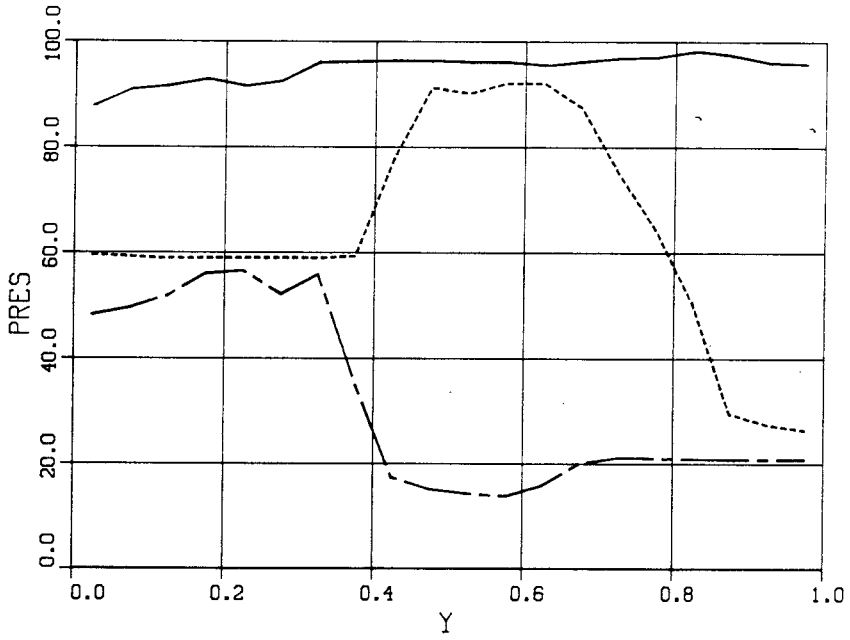

Figure 4a Pressure distribution in the fracture for Run 06 as a function of the y−location. Lines show pressure at x = 0.25 (full line), x = 0.50 (dashed line), and x = 0.75 (chain−dashed line).

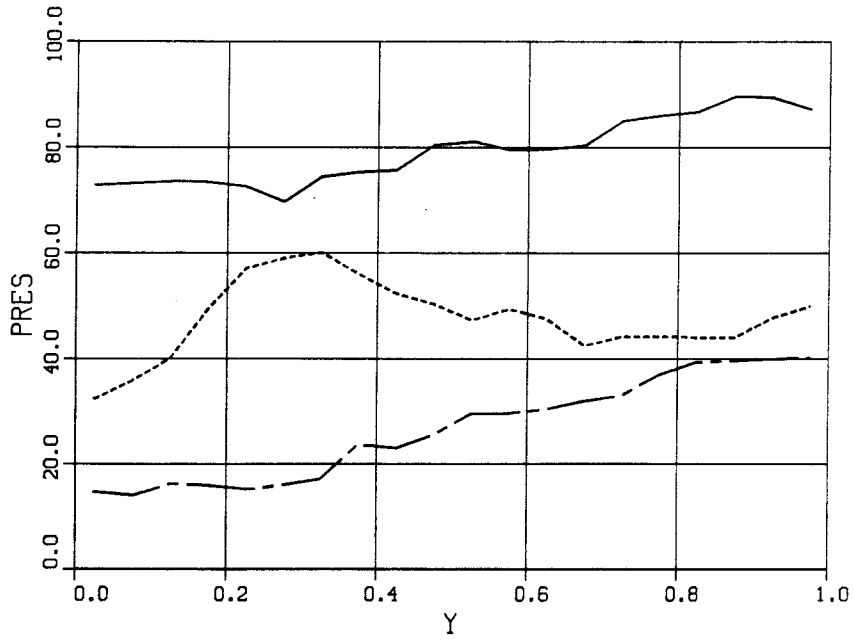

Figure 4b Pressure distribution in the fracture for Run 25 as a function of the y−location. Lines show pressure at x = 0.25 (full line), x = 0.50 (dashed line), and x = 0.75 (chain−dashed line).

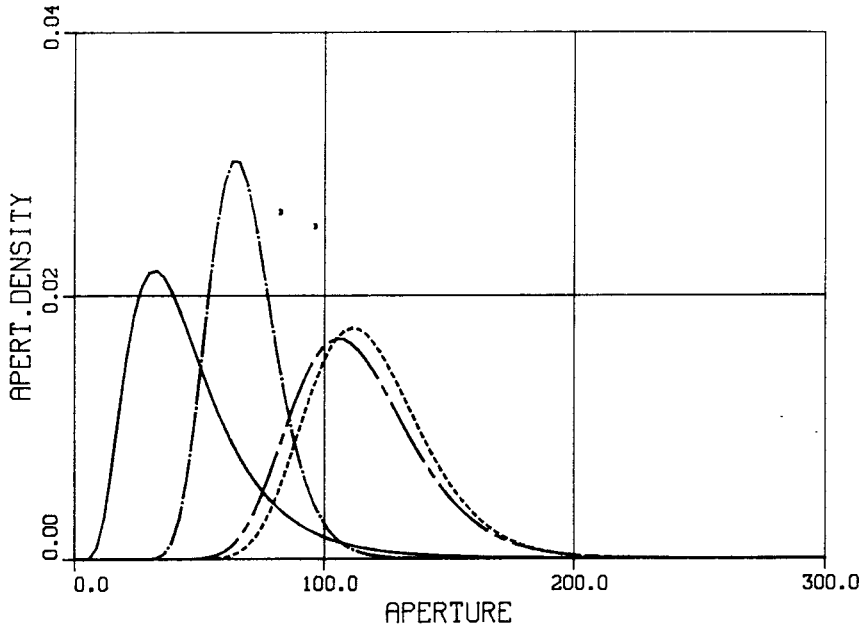

Figure 5 Density function for node apertures in the fracture for Run 06 (full line), for the fastest pathways (dashed line), for the intermediate pathways (chain−dashed line), and for the lowest pathways (chain−dotted line).

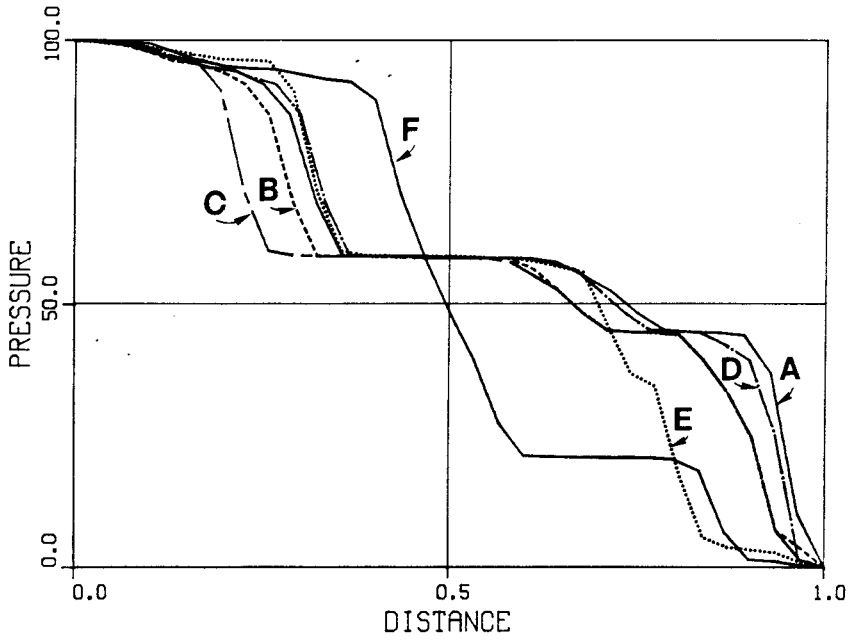

Figure 6 Pressure profiles along some channels (profiles A and B for fast channels, profiles C and D for intermediate channels, and profiles E and F for slow channels).

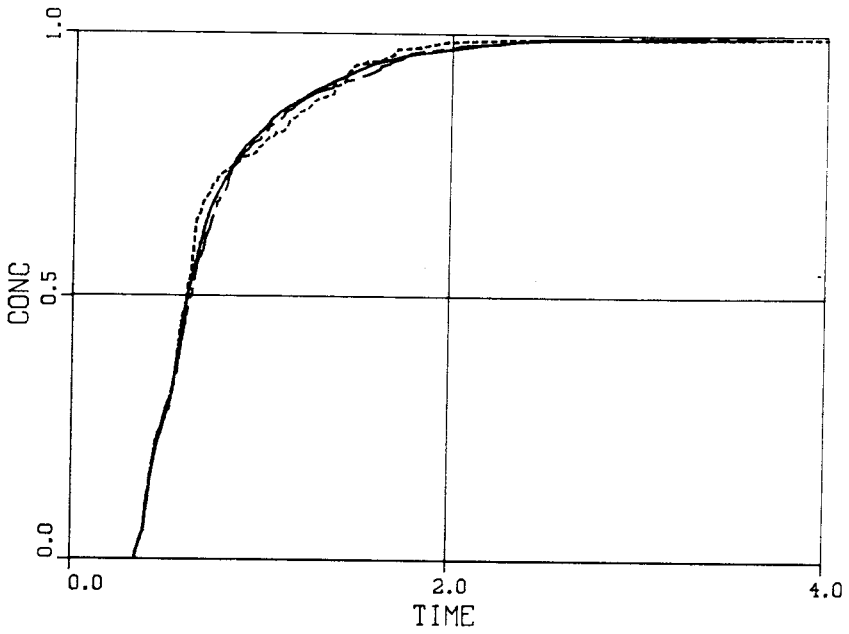

Figure 7 Breakthrough curves for step injection calculated for different number of particles (full line for 3200 particles, chain−dashed line for 400 particles, and dashed line for 200 particles).

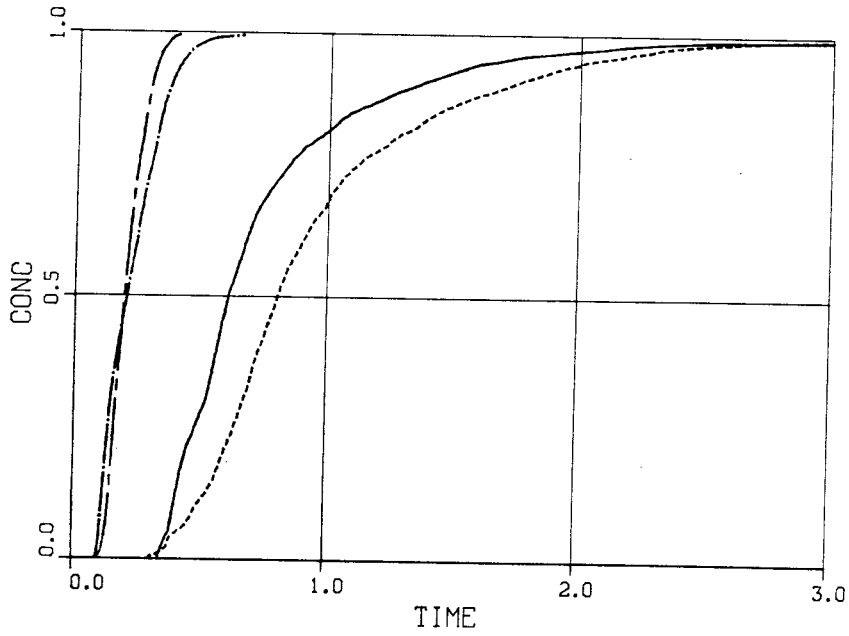

Figure 8 Breakthrough curves for different runs. Run 06 (Full line), Run 18 (Dashed line), Run 34 (Chain−dotted line), and Run 25 (Chain−dashed line).

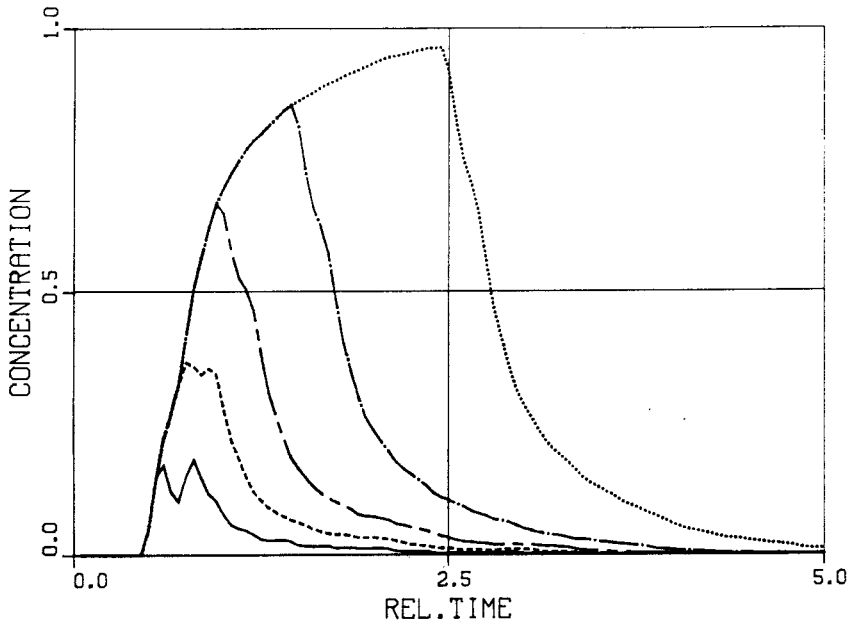

Figure 9 Breakthrough curves for a square pulse injection for different injection times. Injection times used are 2.0 t_w (full line), 1.0 t_w (dashed line), 0.5 t_w (chain−dashed line), 0.25 tw (chain−dotted line), and 0.1 t_w (dotted line).

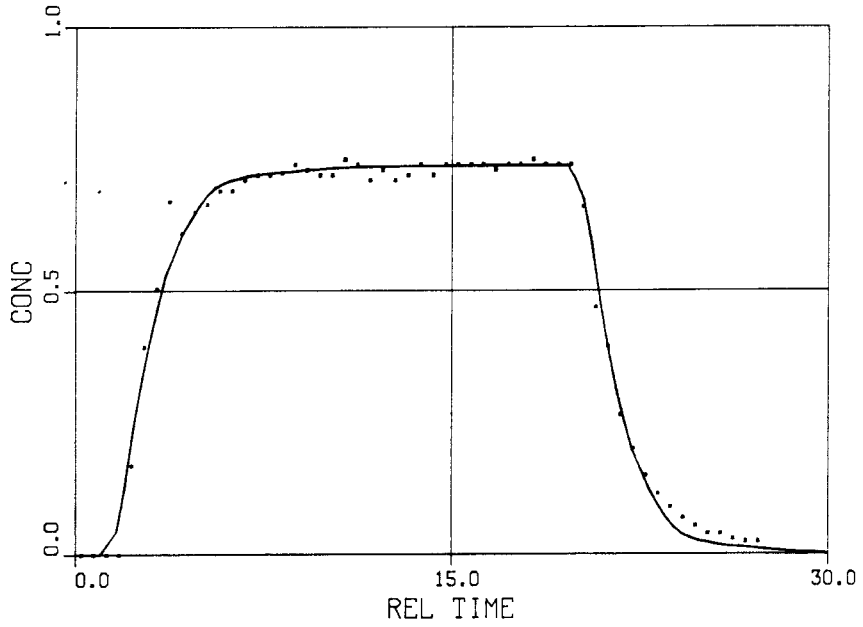

Figure 10 Tracer tests in a fracture in the laboratory. The full line shows a realization with σ = 0.50, λ/L = 0.2, and Δt = 18.5 min (Δt = 5.68 t_w).

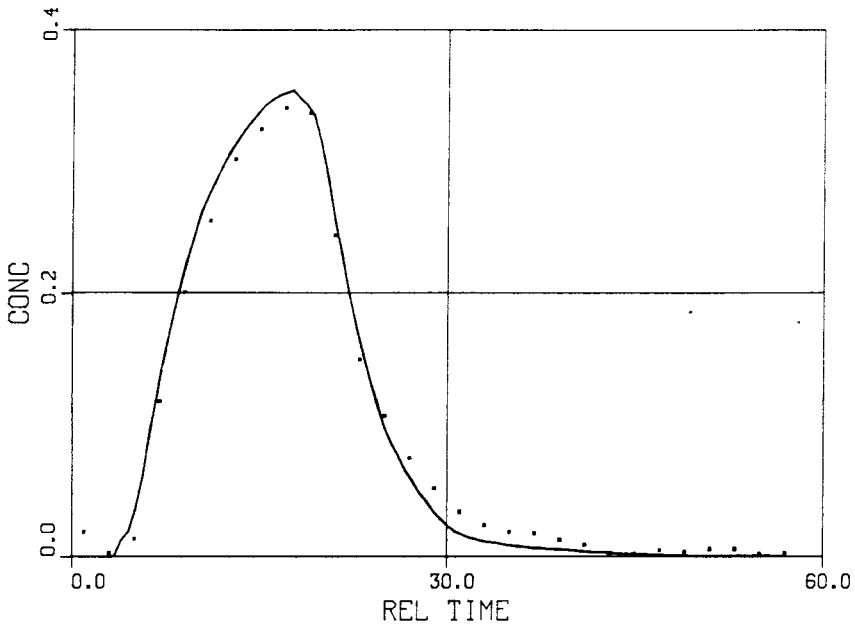

Figure 11 Tracer tests in a fracture in the laboratory. The full line shows a realization with $\sigma = 0.50$, $\lambda/L = 0.2$, and $\Delta t = 14.5$ min ($\Delta t = 1.53\ t_w$).

APPENDIX A

Table A1

Flow properties for different realizations.

Run	σ	σ_o μm	λ/L	n	δ_f [μm]	δ_f/δ_c	Flow(1) [L^3/T]	t_w(1,2) [T]
00	0.50	41.2	0.20	4	57.43	2.02	45.68	1.257
01	0.50	41.2	0.20	4	145.0	1.75	1141.	0.127
02	0.50	41.2	0.20	4	100.2	2.27	172.9	0.580
03	0.50	41.2	0.20	4	57.72	2.23	34.81	1.658
04	0.50	41.2	0.20	4	68.00	1.90	92.36	0.736
05	0.50	41.2	0.20	4	56.32	2.04	42.15	1.336
06	0.50	41.2	0.20	4	69.41	1.95	90.49	0.767
07	0.50	41.2	0.20	4	94.74	3.15	54.48	1.739
08	0.50	41.2	0.20	4	61.33	2.07	51.80	1.184
09	0.50	41.2	0.20	4	64.93	1.66	118.8	0.547
10	0.50	41.2	0.10	2	67.81	2.18	59.81	1.134
11	0.50	41.2	0.10	2	75.40	2.13	88.72	0.850
12	0.50	41.2	0.10	2	90.60	1.90	216.6	0.418
13	0.50	41.2	0.10	2	57.34	2.15	37.95	1.511
14	0.50	41.2	0.10	2	82.26	2.48	73.29	1.122
15	0.50	41.2	0.10	2	71.83	2.24	66.05	1.088
16	0.50	41.2	0.10	2	81.92	2.04	129.9	0.631
17	0.50	41.2	0.10	2	85.93	2.35	97.58	0.881
18	0.50	41.2	0.10	2	71.60	2.15	74.13	0.966
19	0.50	41.2	0.10	2	90.59	1.67	317.5	0.285

Table A1 (cont.)

Run	σ	σ_o μm	λ/L	n	δ_f [μm]	δ_f/δ_c	Flow(1) [L^3/T]	t_w(1,2) [T]
30	0.30	63.0	0.20	4	68.65	1.44	218.2	0.315
31	0.30	63.0	0.20	4	65.51	1.39	210.5	0.311
32	0.30	63.0	0.20	4	75.69	1.50	256.0	0.296
33	0.30	63.0	0.20	4	84.65	1.26	606.6	0.140
34	0.30	63.0	0.20	4	75.32	1.37	329.5	0.230
35	0.30	63.0	0.20	4	55.40	1.30	154.7	0.358
36	0.30	63.0	0.20	4	81.20	1.20	624.0	0.130
37	0.30	63.0	0.20	4	70.85	1.27	343.7	0.206
38	0.30	63.0	0.20	4	97.68	1.25	947.7	0.103
39	0.30	63.0	0.20	4	83.74	1.23	624.0	0.134
20	0.30	63.0	0.10	2	70.97	1.43	243.9	0.291
21	0.30	63.0	0.10	2	77.65	1.35	380.8	0.204
22	0.30	63.0	0.10	2	82.39	1.43	382.0	0.216
23	0.30	63.0	0.10	2	66.69	1.27	290.9	0.229
24	0.30	63.0	0.10	2	75.36	1.36	341.4	0.221
25	0.30	63.0	0.10	2	78.83	1.37	377.6	0.209
26	0.30	63.0	0.10	2	74.47	1.41	295.9	0.252
27	0.30	63.0	0.10	2	71.83	1.46	240.0	0.299
28	0.30	63.0	0.10	2	81.71	1.28	516.9	0.158
29	0.30	63.0	0.10	2	84.98	1.32	533.4	0.159

Table A1 (cont.)

Run	σ	σ_o μm	λ/L	n	δ_f [μm]	δ_f/δ_c	Flow(1) [L^3/T]	t_w(1,2) [T]
40	0.50	41.2	0.20	2	60.15	2.18	42.03	1.431
41	0.50	41.2	0.20	2	83.80	2.17	114.6	0.731
42	0.50	41.2	0.20	2	103.6	2.56	133.5	0.776
43	0.50	41.2	0.20	2	94.57	1.13	1166.	0.081
44	0.50	41.2	0.20	2	59.10	1.96	55.06	1.073
45	0.50	41.2	0.20	2	114.7	1.83	493.4	0.232
46	0.50	41.2	0.20	2	109.2	2.17	255.8	0.427
47	0.50	41.2	0.20	2	46.95	2.51	13.16	3.568
48	0.50	41.2	0.20	2	72.32	2.35	58.42	1.238
49	0.50	41.2	0.20	2	58.62	1.60	97.41	0.602
50	0.50	41.2	0.10	4	70.82	2.14	72.09	0.982
51	0.50	41.2	0.10	4	79.20	1.96	133.0	0.595
52	0.50	41.2	0.10	4	88.64	2.00	174.0	0.509
53	0.50	41.2	0.10	4	92.83	1.65	358.2	0.259
54	0.50	41.2	0.10	4	66.95	2.05	70.00	0.956
55	0.50	41.2	0.10	4	74.86	2.07	95.20	0.786
56	0.50	41.2	0.10	4	61.27	2.00	57.59	1.064
57	0.50	41.2	0.10	4	76.89	2.13	93.96	0.818
58	0.50	41.2	0.10	4	77.67	2.67	49.03	1.584
59	0.50	41.2	0.10	4	58.57	2.97	15.30	3.828

(1) Arbitrary units

(2) Calculated from fracture volume/flow

Table A2

Transport properties for different realizations.

Run	σ	σ_o μm	λ/L	n	t_w(1,2) [T]	Pe(2)	Pe(3)
00	0.50	41.2	0.20	4	1.271	3.47	8.5
01	0.50	41.2	0.20	4	0.130	1.38	6.8
02	0.50	41.2	0.20	4	0.577	7.23	17.5
03	0.50	41.2	0.20	4	1.636	4.01	4.2
04	0.50	41.2	0.20	4	0.741	8.29	8.0
05	0.50	41.2	0.20	4	1.346	2.16	2.5
06	0.50	41.2	0.20	4	0.764	4.64	6.0
07	0.50	41.2	0.20	4	1.746	4.95	6.7
08	0.50	41.2	0.20	4	1.189	7.04	5.7
09	0.50	41.2	0.20	4	0.560	1.61	6.2
10	0.50	41.2	0.10	2	1.132	11.63	11.0
11	0.50	41.2	0.10	2	0.849	3.41	6.2
12	0.50	41.2	0.10	2	0.417	4.95	12.5
13	0.50	41.2	0.10	2	1.519	7.77	10.5
14	0.50	41.2	0.10	2	1.118	4.99	4.1
15	0.50	41.2	0.10	2	1.078	8.07	13.5
16	0.50	41.2	0.10	2	0.630	2.15	15.5
17	0.50	41.2	0.10	2	0.879	11.27	11.8
18	0.50	41.2	0.10	2	0.960	6.93	6.2
19	0.50	41.2	0.10	2	0.288	0.86	8.3

Table A2 (cont.)

Run	σ	σ_o μm	λ/L	n	t_w(1,2) [T]	Pe(2)	Pe(3)
30	0.30	63.0	0.20	4	0.315	21.10	20.5
31	0.30	63.0	0.20	4	0.310	16.38	24.5
32	0.30	63.0	0.20	4	0.295	14.58	12.5
33	0.30	63.0	0.20	4	0.138	10.94	20.5
34	0.30	63.0	0.20	4	0.228	9.35	9.0
35	0.30	63.0	0.20	4	0.358	15.48	13.0
36	0.30	63.0	0.20	4	0.130	10.61	22.0
37	0.30	63.0	0.20	4	0.207	9.59	8.5
38	0.30	63.0	0.20	4	0.103	11.44	18.0
39	0.30	63.0	0.20	4	0.135	26.95	33.5
20	0.30	63.0	0.10	2	0.291	31.37	30.5
21	0.30	63.0	0.10	2	0.205	22.22	22.5
22	0.30	63.0	0.10	2	0.215	21.38	19.5
23	0.30	63.0	0.10	2	0.228	12.77	13.0
24	0.30	63.0	0.10	2	0.221	12.50	14.0
25	0.30	63.0	0.10	2	0.208	24.00	23.0
26	0.30	63.0	0.10	2	0.252	37.34	39.5
27	0.30	63.0	0.10	2	0.300	43.36	42.0
28	0.30	63.0	0.10	2	0.157	9.12	9.0
29	0.30	63.0	0.10	2	0.160	13.46	13.0

Table A2 (cont.)

Run	σ	σ_o μm	λ/L	n	t_w(1,2) [T]	Pe(2)	Pe(3)
40	0.50	41.2	0.20	2	1.454	4.80	4.4
41	0.50	41.2	0.20	2	0.724	1.73	14.0
42	0.50	41.2	0.20	2	0.774	6.34	16.8
43	0.50	41.2	0.20	2	0.094	0.18	8.2
44	0.50	41.2	0.20	2	1.068	5.51	26.0
45	0.50	41.2	0.20	2	0.234	3.45	3.5
46	0.50	41.2	0.20	2	0.424	3.09	3.0
47	0.50	41.2	0.20	2	3.515	12.21	19.0
48	0.50	41.2	0.20	2	1.234	2.26	15.6
49	0.50	41.2	0.20	2	0.600	7.32	15.8
50	0.50	41.2	0.10	4	1.005	3.35	2.6
51	0.50	41.2	0.10	4	0.601	8.38	11.8
52	0.50	41.2	0.10	4	0.500	3.32	3.4
53	0.50	41.2	0.10	4	0.258	3.38	3.7
54	0.50	41.2	0.10	4	0.951	6.79	7.0
55	0.50	41.2	0.10	4	0.786	3.17	4.6
56	0.50	41.2	0.10	4	1.057	4.60	4.9
57	0.50	41.2	0.10	4	0.820	6.22	11.2
58	0.50	41.2	0.10	4	1.597	9.68	13.2
59	0.50	41.2	0.10	4	3.820	12.47	16.6

(1) Arbitrary units

(2) Calculated using moments

(3) Calculated from $(t_{0.9}-t_{0.1})/t_{0.5}$

List of SKB reports

Annual Reports

1977–78
TR 121
KBS Technical Reports 1 – 120.
Summaries. Stockholm, May 1979.

1979
TR 79–28
The KBS Annual Report 1979.
KBS Technical Reports 79-01 – 79-27.
Summaries. Stockholm, March 1980.

1980
TR 80–26
The KBS Annual Report 1980.
KBS Technical Reports 80-01 – 80-25.
Summaries. Stockholm, March 1981.

1981
TR 81–17
The KBS Annual Report 1981.
KBS Technical Reports 81-01 – 81-16.
Summaries. Stockholm, April 1982.

1982
TR 82–28
The KBS Annual Report 1982.
KBS Technical Reports 82-01 – 82-27.
Summaries. Stockholm, July 1983.

1983
TR 83–77
The KBS Annual Report 1983.
KBS Technical Reports 83-01 – 83-76
Summaries. Stockholm, June 1984.

1984
TR 85–01
Annual Research and Development Report 1984
Including Summaries of Technical Reports Issued during 1984. (Technical Reports 84-01– 84-19)
Stockholm June 1985.

1985
TR 85-20
Annual Research and Development Report 1985
Including Summaries of Technical Reports Issued during 1985. (Technical Reports 85-01-85-19)
Stockholm May 1986.

1986
TR 86-31
SKB Annual Report 1986
Including Summaries of Technical Reports Issued during 1986
Stockholm, May 1987

1987
TR 87-33
SKB Annual Report 1987
Including Summaries of Technical Reports Issued during 1987
Stockholm, May 1988

Technical Reports

1988
TR 88-01
Preliminary investigations of deep ground water microbiology in Swedish granitic rocks
Karsten Pedersen
University of Göteborg
December 1987

TR 88-02
Migration of the fission products strontium, technetium, iodine, cesium and the actinides neptunium, plutonium, americium in granitic rock
Thomas Ittner[1], Börje Torstenfelt[1], Bert Allard[2]
[1]Chalmers University of Technology
[2]University of Linköping
January 1988